# Ultrafast carrier response of $Br^+$-irradiated $In_{0.53}Ga_{0.47}As$ excited at telecommunication wavelengths

L. Fekete,[1] H. Němec,[1] Z. Mics,[1] F. Kadlec,[1] P. Kužel,[1,a)] V. Novák,[2] J. Lorinčík,[3,4] M. Martin,[5] J. Mangeney,[5] J. C. Delagnes,[6] and P. Mounaix[6]
[1]*Institute of Physics, ASCR, Na Slovance 2, 182 21 Prague 8, Czech Republic*
[2]*Institute of Physics ASCR, Cukrovarnická 10, 162 53 Prague 6, Czech Republic*
[3]*Institute of Photonics and Electronics ASCR, Chaberská 57, 18251 Prague 8, Czech Republic*
[4]*Department of Physics, Faculty of Science, J.E. Purkinje University, Ceske mladeze 8, 40096, Usti nad Labem, Czech Republic*
[5]*Institut d'Electronique Fondamentale, Université Paris XI, UMR CNRS 8622, 91405 Orsay Cedex, France*
[6]*Laboratoire Ondes et Matière d'Aquitaine, Université Bordeaux I, UMR CNRS 5798, 351 Cours de la Libération, 33405 Talence Cedex, France*

(Received 7 December 2011; accepted 27 March 2012; published online 10 May 2012)

We present results of infrared pump—terahertz probe experiments applied to a set of $In_{0.53}Ga_{0.47}As$ films irradiated with heavy ions ($Br^+$) at doses from $10^9$ to $10^{12}\,cm^{-2}$. Photoexcitation at 1400 nm (0.89 eV) allowed us to characterize the response close to telecommunications' wavelengths whilst avoiding the intervalley carrier scattering observed when a shorter wavelength excitation is used. The excitation fluence was varied in our experiments in order to characterize the dynamics in detail: the lifetimes and mobilities of both electrons and holes were retrieved, and the trap filling and carrier diffusion were clearly observed. The $In_{0.53}Ga_{0.47}As$ film irradiated by the dose of $10^{12}\,cm^{-2}$ exhibits simultaneously ultrashort electron lifetime (~300 fs) and very high electron mobility (2800 $cm^2V^{-1}s^{-1}$). These findings are particularly important for the design of terahertz emitters controlled by lasers operating at standard telecommunication wavelengths. © *2012 American Institute of Physics*. [http://dx.doi.org/10.1063/1.4709441]

## I. INTRODUCTION

In terahertz time-domain experiments and devices, the opto-electronic approach to the generation of pulsed radiation is typically based on optical rectification in nonlinear crystals—such as non-centrosymmetric semiconductors like GaAs, or ZnTe (Refs. 1 and 2)—or on photoswitching in ultrafast semiconductors, e.g., in low-temperature-grown GaAs.[3,4] The choice of materials has been largely dictated by the availability of Ti:sapphire femtosecond laser systems, which operate at wavelengths near 800 nm. A promising alternative to this rather robust approach is a combination of less expensive femtosecond lasers operating at the telecommunication wavelength of 1.55 $\mu$m on the one hand, and ultrafast semiconductors based on InGaAs (Ref. 5) or organic crystals like 4-dimethylamino-N-methyl-4-stilbazolium tosylate (DAST)[6] on the other hand. DAST is mainly used in broadband THz setups.[7] However, the THz spectrum emitted from a DAST crystal is compromised due to the presence of a phonon mode at 1.1 THz.[8]

Materials suitable for efficient generation of THz radiation by photoswitching should fulfill the following requirements: (1) subpicosecond carrier lifetime, (2) high photocarrier mobility, and (3) high dark electrical resistivity. However, simultaneous optimization of these parameters is a complex task, as it requires a feedback between material growth technologies, the investigation of ultrafast carrier dynamics and the emitter preparation and testing.

Among the ultrafast semiconductors with a low band gap, $In_{0.53}Ga_{0.47}As$ ($E_g = 0.74$ eV) is a promising candidate for THz photoswitches driven by radiation at wavelengths as long as 1.67 $\mu$m. In this context, Be-doped low-temperature-grown InGaAs,[9] InGaAs film with embedded ErAs nanoislands,[10] Fe-doped InGaAs,[11] $Fe^+$ ion,[12] and heavy ion irradiated InGaAs materials were investigated in the past, and (sub)picosecond photocarrier response in these materials was achieved.

In this paper, we use an infrared pump—THz probe technique to study the ultrafast dynamics of electrons and holes in $In_{0.53}Ga_{0.47}As$ films grown on InP substrates and irradiated by $Br^+$ ions at high energies. This material was already tested for THz emission and detection in conjunction with excitation at 800 nm and 1.55 $\mu$m wavelengths.[13,14] However, in those experiments, only limited information about the ultrafast response of the material was obtained. A more detailed study of the material response was carried out in our previous work;[15] however, due to photoexcitation at 800 nm, intervalley carrier scattering strongly affected the dynamics of electrons on the ultrafast time-scale.[16] In the current work, we avoid intervalley scattering by using low excess energies of ~140 meV (photoexcitation at 1.4 $\mu$m wavelength). The band structure of $In_{0.53}Ga_{0.47}As$ taken from Ref. 17, and the photoexcitation pathways are shown in Fig. 1. This allows us to assess directly the ultrafast photoelectron dynamics in InGaAs in the regime of its potential application as a THz emitter driven by telecom lasers. We take advantage of these experimental conditions to perform a detailed study of the dynamics with a variable initial carrier

a)E-mail: kuzelp@fzu.cz.

 © 2012 American Institute of Physics

Downloaded 10 May 2012 to 147.231.27.153. Redistribution subject to AIP license or copyright; see http://jap.aip.org/about/rights_and_permissions

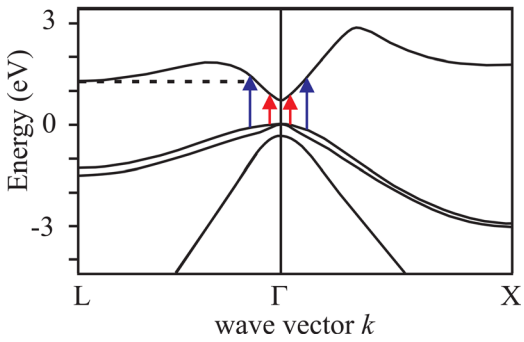


FIG. 1. Band structure of $In_{0.53}Ga_{0.47}As$, taken from Ref. 17. The red arrows represent photoexcitation at 1400 nm, the blue arrows at 800 nm; the dotted line marks the energy of the *L*-valley minimum.

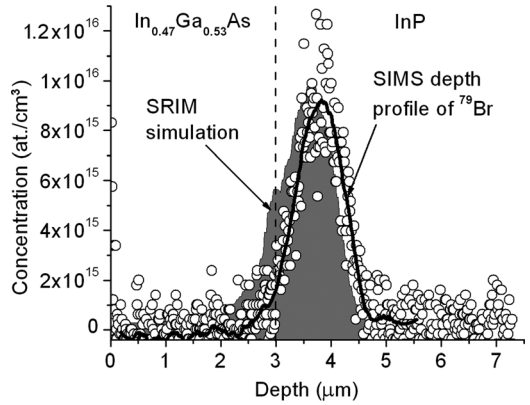


FIG. 2. Depth profile of calculated (SRIM) and measured (SIMS) Br-ion implantation densities.

concentration in order to evaluate simultaneously the free-electron and hole lifetimes and to determine the density of traps.

## II. SAMPLES

The undoped 3-$\mu$m-thick $In_{0.53}Ga_{0.47}As$ layers were grown using gas source molecular-beam-epitaxy on a lattice-matched semi-insulating InP:Fe substrate. After the growth, the films were irradiated by 11 MeV $Br^+$ ions at four different doses of $10^9$, $10^{10}$, $10^{11}$, and $10^{12}\,cm^{-2}$; these samples are denoted A, B, C, and D, respectively, and they are actually identical to the samples investigated in Ref. 15, where the same notation was used.

For the estimation of the damage profiles produced by the $Br^+$ irradiation, a "Stopping Range of Ions in the Matter" (SRIM) software was used;[18] and these theoretical results were checked by secondary ion mass spectroscopy (SIMS) measurements for the most irradiated sample (D). Negative secondary ion $^{79}Br^-$ depth profile data were acquired using Atomika 3000 secondary ion mass spectrometer. The sample was bombarded with primary ion beam of 10 keV $Cs^+$ at impact angle 45° (ion current 210 nA, 500 $\mu$m raster, acceleration voltage 200 V, energy window ~10 eV, vacuum pressure $2 \times 10^{-9}$ Torr). The depth scale was calibrated from a mechanical stylus profilometer measurement of the SIMS crater using the known thickness of the $In_{0.47}Ga_{0.53}As$ layer. From the Br implantation dose, the raw data in counts/s were converted to concentration in at./cm$^3$. The agreement of both the shift and the height of the implantation profile between the experiment and the SRIM simulation are within the estimated experimental uncertainties of ~10% and ~20%, respectively (see Fig. 2).

According to these results, the energy of bromine ions is too high to allow implantation of Br atoms in the thin InGaAs layer. Instead, $Br^+$ ions are stopped further along their path in the InP:Fe substrate leaving the lattice of the InGaAs layer damaged exclusively due to host-atom displacements. Complete depth profiles of the calculated densities of host-atom displacement defects and implantation densities of Br-atoms were published in Ref. 19; we denote the calculated concentration of host-atom displacements near the outer surface of the film as $n_{host}$. In $Br^+$ irradiated InGaAs samples, two main types of defects are created:[20] the majority of defects consist of defect clusters with neutral charge and deep energy levels; a smaller concentration of ionized point defects with shallow energy levels is also present. Both kinds of defects act as traps and recombination and scattering centers reducing the free carrier lifetime and the momentum scattering time. For $Br^+$-irradiated InGaAs samples, the host-atom density of defects is expected to be proportional to the irradiation dose.

All the investigated samples were characterized by DC resistivity and Hall effect measurements. To eliminate the contribution of the substrate conductance, samples of substrates (obtained by etching-off the InGaAs films) were measured independently and used to decompose the transport parameters of the combined structures.[21] The resulting Hall mobilities and sheet resistivities of the InGaAs layers are summarized in Table I. The residual electron density is in the range of $1–2 \times 10^{15}\,cm^{-1}$ for all the samples studied.

## III. EXPERIMENTAL METHOD

Transient THz conductivity spectra of InGaAs films were obtained by an optical (infrared) pump—THz probe

TABLE I. Sheet resistivity $\rho_{sheet}$ and Hall mobility $\mu_{Hall}$ obtained by DC resistivity and Hall measurements (~10% experimental error); scattering time $\tau_{s,e}$ and mobility $\mu_e$ obtained by fitting the transient conductivity spectra with the Drude formula Eq. (1) for the specified range of initial carrier concentrations $n_0$ (values obtained from the fit).

| Sample | $\rho_{sheet}$ (kΩ) | $\mu_{Hall}$ ($cm^2V^{-1}s^{-1}$) | $n_0$ range ($10^{15}\,cm^{-3}$) | $\tau_{s,e}$ (fs) | $\mu_e$ ($cm^2V^{-1}s^{-1}$) |
|---|---|---|---|---|---|
| A | 1.1 | 9100 | 0.4–55 | 230 ± 30 | 10 000 ± 1300 |
| B | 1.8 | 8200 | 1–55 | 230 ± 30 | 10 000 ± 1300 |
| C | 4.1 | 4600 | 1–130 | 160 ± 25 | 7000 ± 1100 |
| D | 16.4 | 870 | 60 | 65 ± 10 | 2800 ± 400 |

Downloaded 10 May 2012 to 147.231.27.153. Redistribution subject to AIP license or copyright; see http://jap.aip.org/about/rights_and_permissions

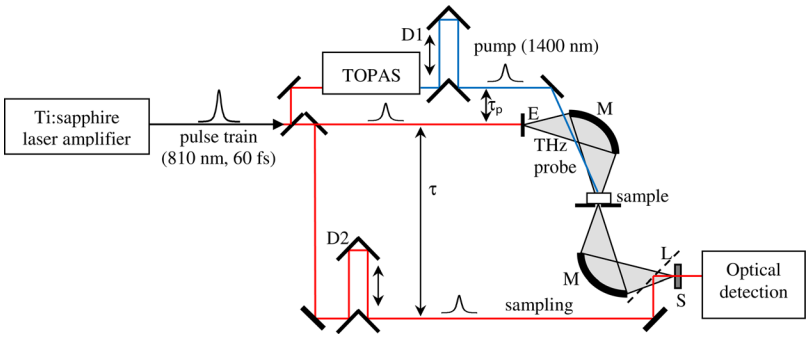


FIG. 3. Scheme of the experimental setup in non-collinear for time-resolved THz spectroscopy. D1—motorized stage for controlling the pump-probe delay ($\tau_p$), TOPAS—optical parametric amplifier, E—emitter (ZnTe crystal), M—ellipsoidal mirrors, D2—motorized stage for scanning the THz pulse profile, L—pellicle beam-splitter, S—sensor (ZnTe crystal).

experimental technique.[22] The experimental setup is shown in Fig. 3. As a source of femtosecond laser pulses, we used a Ti:sapphire laser amplifier (Quantronix, Odin) with a 1 kHz repetition rate providing 60 fs pulses with a mean wavelength of 810 nm and an energy of 1 mJ per pulse. The pulse train was split into three branches, each one equipped with a delay line to control the arrival of the pulses to the experiment. The first branch served for the generation of terahertz pulses via optical rectification in a 1-mm-thick [011] ZnTe crystal. The second branch was used to gate the electro-optic detection in another [011] ZnTe crystal for phase-sensitive measurement of the time profile $E(\tau)$ of the transmitted THz field. The third branch was used for the optical excitation of samples and involved an optical parametric amplifier (TOPAS) to obtain a train of optical pump pulses at 1.4 $\mu$m. We used slightly noncollinear pump–probe geometry for the investigation of samples A, B, and C, for which the photoconductive response varies on the time scale of units to hundreds of picoseconds. The oblique incidence of the excitation beam causes a lower experimental time resolution, ~1.5 ps. A collinear setup, allowing one to achieve subpicosecond time resolution, was used to measure the ultrafast dynamics of sample D. Further details about these experimental arrangements were provided in Ref. 22. The whole terahertz setup was enclosed in a vacuum box to avoid the water vapor absorption.

The pump beam spot on the sample significantly exceeded the area probed by the THz beam in order to achieve homogeneous excitation. For samples A, B, and C experiments with variable pump fluence were performed in the linear absorption regime: gray filters were used to attenuate the pump beam in order to achieve a variable concentration of photoexcited carriers in the range of about $5 \times 10^{14}$–$1 \times 10^{17}$ cm$^{-3}$. The penetration depth of the 1.4 $\mu$m excitation beam is about 900 nm;[23] under this condition the pump beam is entirely absorbed within the InGaAs thin film.

We measured the time profile $E_{\mathrm{ref}}(\tau)$ of the THz pulse transmitted through the unexcited sample and its absolute change $\Delta E(\tau,\tau_p)$ induced by the photoexcitation, for several pump–probe delay times $\tau_p$.[22] From these data, we evaluated the transient conductivity spectra $\Delta\sigma(\omega,\tau_p)$ of samples A, B, and C in the quasi-steady-state approximation as described in Ref. 22. This approximation involves the assumption that the state of the photoexcited sample does not change during the probing event.

In the case of the sample D, where the dynamics occur on a subpicosecond time scale, i.e., faster than the THz pulse duration, the pump-probe data $\Delta E(\tau,\tau_p)$ were measured on a two-dimensional grid of $90 \times 54$ points with a step of 70 fs in both directions (i.e., the grid fits within a rectangle of 6.3 ps $\times$ 3.8 ps). The transient conductivity spectra in the Fourier space of the pump–probe delay,

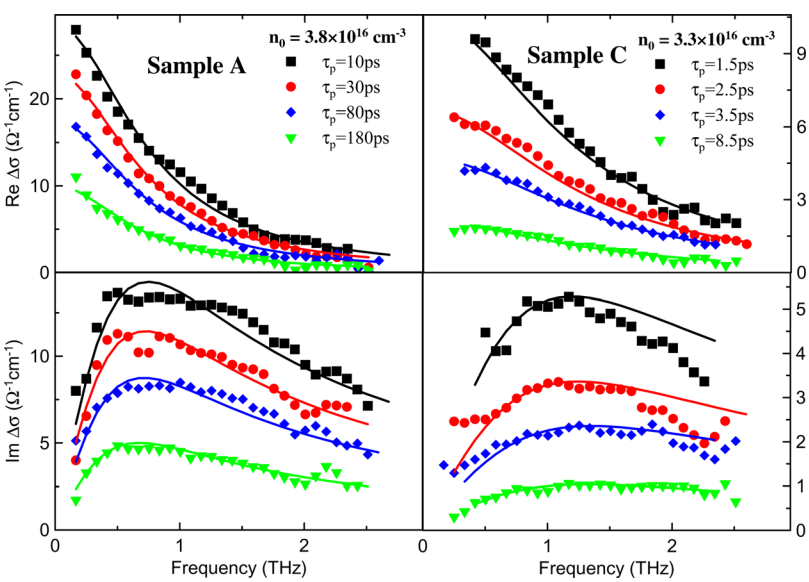


FIG. 4. Complex transient conductivity spectra: experimental data (symbols) and the Drude fit (lines) for sample A (left) and sample C (right).

Downloaded 10 May 2012 to 147.231.27.153. Redistribution subject to AIP license or copyright; see http://jap.aip.org/about/rights_and_permissions

$\Delta\sigma(\omega,\omega_p)$, were then calculated, see Refs. 22 and 24 for further details.

In addition, THz kinetics representing the evolution of spectrally averaged THz photoconductivity versus pump–probe delay was obtained for samples A, B, and C. Here, the maximum of the transient terahertz waveform $\Delta E(\tau_{max},\tau_p)$ was directly recorded as a function of $\tau_p$. Subsequently, we measured a series of waveforms $\Delta E(\tau,\tau_p)$ for a few pump-probe delays $\tau_p$ under the same experimental conditions. Their interpolation with a weight $\Delta E(\tau_{max},\tau_p)$ was then used to evaluate the spectra $\Delta E(\omega,\tau_p)$ for any $\tau_p$ and hence we obtained the time-evolution of spectra of the transient conductivity $\Delta\sigma(\omega,\tau_p)$. The results of such measurements will be discussed in Sec. V.

## IV. SPECTRAL RESPONSE

The transient conductivity spectra of samples A, B, and C were fitted using the Drude formula for conductivity due to one type of free carriers (see Fig. 4). This approximation can be applied for short or medium pump–probe delays as electrons are significantly more mobile than holes. The Drude formula for the electrons then reads

$$\Delta\sigma(\omega,\tau_p) = n(\tau_p)e_0\frac{\mu_e}{1-i\omega\tau_{s,e}}. \quad (1)$$

Here, $e_0$ is the elementary charge, $n(\tau_p)$ is the free electron density exhibiting decay due to trapping and recombination, and $\tau_{s,e}$ is the electron momentum relaxation time. The term $\mu_e = e_0\tau_{s,e}/m_{eff}$ is the dc photoelectron mobility (the effective mass of electrons in $In_{0.53}Ga_{0.47}As$ at the bottom of Γ-valley is $m_{eff} = 0.041\,m_e$ (Ref. 25)). Fitting the transient conductivity spectra with the Drude term yields values of $\tau_{s,e}$ and $\mu_e$. The scattering time $\tau_s$ was found to be independent of the carrier density for the range of pump fluences used. The initial carrier concentration $n_0 \equiv n(0)$ obtained from the fit was found to be about twice as small as that estimated from the measured incident pump photon flux which is a reasonable agreement. The values are summarized in Table I.

The sample D irradiated with the highest dose exhibits subpicosecond carrier lifetime. A two-dimensional spectral map of the transient photoconductivity $\Delta\sigma(\omega,\omega_p)$ is displayed in Figs. 5(a), 5(c), and 5(e). The monotonous decrease of the amplitude of the photoinduced conductivity $\Delta\sigma(\omega,\omega_p)$ along the $\omega$ axis, observed in Fig. 5(e), indicates the Drude response of the carriers.[26] The marked decrease of conductivity with increasing $|\omega_p|$ is a clear signature of ultrashort carrier lifetime. To fit the data, we assumed exponential decay of the free carrier concentration with the lifetime $\tau_c$[26,27]

$$\Delta\sigma(\omega,\omega_p) = \frac{n_0e_0^2\tau_{s,e}}{m_{eff}}\cdot\frac{1}{1+\frac{\tau_{s,e}}{\tau_c}-i\omega\tau_{s,e}}\cdot\frac{1}{\frac{1}{\tau_c}-i\omega_p}. \quad (2)$$

This expression was used to simultaneously fit the real and imaginary parts of the experimental data [Figs. 5(a)–5(d)]. The featureless residuals of the fit displayed in Fig. 5(f) indicate a very good agreement between the measured data and the model. The parameters $\tau_{s,e}$ and $n_0$ are provided in

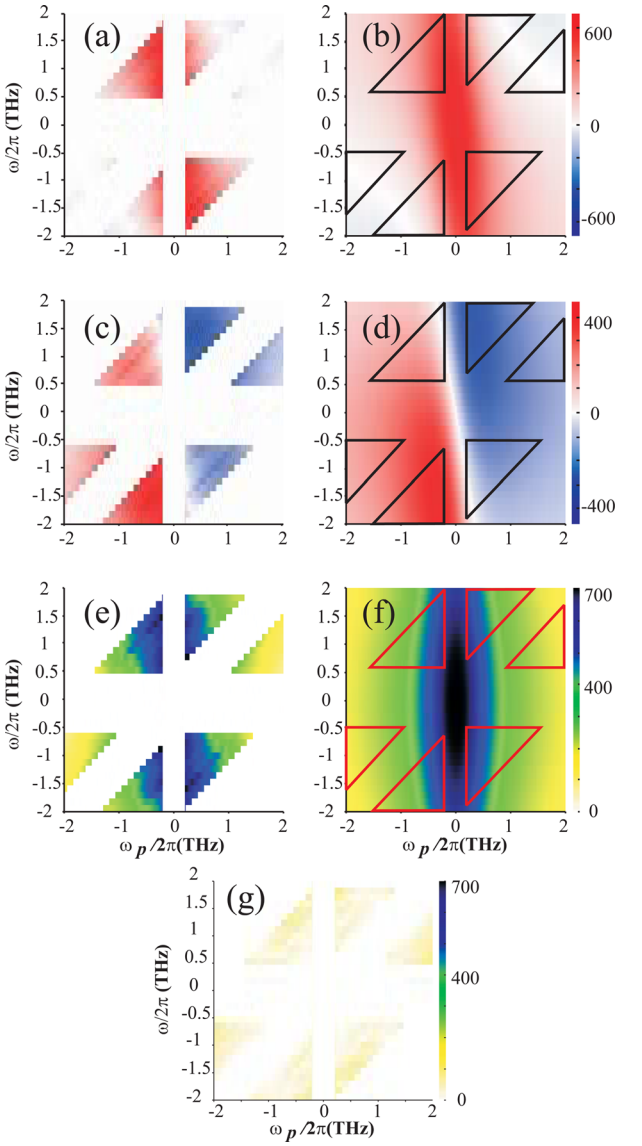


FIG. 5. Transient conductivity spectra of the sample D in the two-dimensional frequency domain (in $\Omega^{-1}$ $THz^{-1}$ $m^{-1}$). (a) real part measured and (b) fitted, respectively; (c) and (d) imaginary part measured and fitted, respectively; (e) and (f) amplitude of the complex conductivity measured and fitted, respectively; and (g) residuals of a complex fit. The complex fitting was done by using Eq. (2) which assumes an exponential decay of the free carrier concentration with the lifetime $\tau_c$.

Table I; the carrier lifetime was found to be $\tau_c = 300$ fs. Note that this short carrier lifetime is accompanied by a relatively high photocarrier mobility of 2800 $cm^2V^{-1}s^{-1}$. For comparison, in $In_{0.53}Ga_{0.47}As$ films with embedded ErAs nanoislands a lifetime of about 3 ps was found by time-resolved THz spectroscopy and the reported Hall mobility was ~400 $cm^2V^{-1}s^{-1}$. In $In_{0.53}Ga_{0.47}As$:ErAs superlattices, the picosecond carrier lifetime can be also substantially decreased by additional Be-doping.[28] A lifetime as low as 300 fs was found for high Be-doping levels,[28] while the Hall mobility of electrons in this case decreased to a value of the order of hundreds $cm^2V^{-1}s^{-1}$.[29]

Finally, we comment on the difference between the Hall mobility and the mobility of photoexcited electrons which are provided in the 3 rd and 6th columns of Table I. The Hall

Downloaded 10 May 2012 to 147.231.27.153. Redistribution subject to AIP license or copyright; see http://jap.aip.org/about/rights_and_permissions

mobility is a low electric field mobility obtained with low densities of carriers ($10^{15}$ cm$^{-3}$), whereas the mobility resulting from our THz measurements is a single carrier response function of photoexcited electrons measured at higher concentrations. In samples with a large density of defects some equilibrium (dark) carriers can spend a large amount of time in lower-mobility states during the measurements while at the early stages after their creation, the large majority of photoexcited electrons are highly mobile. Therefore, the defect scattering due to irradiation process affects more the Hall mobility as deduced from Table I.

## V. DYNAMICS OF ELECTRONS AND HOLES

Here, we report the experimental data representing the evolution of THz photoconductivity versus pump–probe delay. Experimentally, we found out that the dynamics of the carrier population depend on the initial carrier concentration and on the concentration of traps created by the $Br^+$ irradiation. For samples A, B, and C, we observed a slowing down of the measured kinetics by a factor of about 1.2–2 within the range of the pump fluence used in our experiments. We attribute this effect to trap filling and to carrier diffusion in the direction perpendicular to the surface.

In the first approximation and in order to compare the dynamics of the samples A, B, and C, the decay times $\tau_c$ were estimated from the fits by a single-exponential decay of the carrier concentration for each individual pump fluence $\phi$: $n(\tau_p,\phi) = n_0(\phi)\exp(-\tau_p/\tau_c)$. For the sample A, $\tau_c$ increases with increasing excitation intensities from 116 to 185 ps; for sample B, we find an increase of $\tau_c$ from 23 to 28 ps; and for sample C, $\tau_c$ increases from 1.5 to 3 ps.

The electron diffusion length is defined as

$$l_D \approx \sqrt{\frac{k_B T \tau_s}{m_{eff}}}\tau_c, \tag{3}$$

where $T$ is the carrier temperature and $k_B$ is the Boltzmann constant. In this way, we obtain the following estimations for sample A: $l_D = 1.7$–$2.2$ $\mu$m, B: $l_D = 0.75$–$0.85$ $\mu$m, and C: $l_D = 0.16$–$0.22$ $\mu$m. This implies that for samples A and B, the diffusion length is longer than or comparable to the absorption length of the excitation beam (0.9 $\mu$m). A significant part of the photogenerated carriers may thus diffuse away from regions close to the sample input surface (where, for high pump fluences, the traps may become filled soon after photoexcitation) into deeper regions of the layer where the traps are nearly empty. In the case of sample C, where the electron diffusion length is smaller than the penetration depth of the excitation light, the kinetics is expected to be mainly determined by the trap filling and the depletion via the recombination of carriers.

To model the dynamics of electrons and holes in more detail, we adopted the model successfully used for the description of ultrafast carrier dynamics in $Br^+$-irradiated InP.[19] The model consists of a set of coupled kinetic equations which involve both the trap filling effect and the diffusion perpendicular to the sample surface (steepest gradient along the $z$-direction). The densities of free electrons ($n_e$), trapped electrons ($n_t$), and free holes ($n_h$) become inhomogeneous and depend on $z$. The model contains six important unknown parameters: the density of traps ($N_t$), the position of trap levels below the conduction band minimum ($E_t$), the lifetime of electrons ($\tau_e$) and that of holes ($\tau_h$), and the scattering time of electrons and holes ($\tau_{s,e}$ and $\tau_{s,h}$); the diffusion coefficient of electrons (holes) is assumed to be given by the Einstein relation $D_{e,h} = k_B T \mu_{e,h}/e_0$.

$$\begin{aligned}
\frac{\partial n_e}{\partial t} &= D_e \frac{\partial^2 n_e}{\partial z^2} - \frac{n_e}{\tau_e}\left(1 - \frac{n_t}{N_t}\right) + g_e n_t \\
\frac{\partial n_t}{\partial t} &= \frac{n_e}{\tau_e}\left(1 - \frac{n_t}{N_t}\right) - \frac{n_h}{\tau_h}\cdot\frac{n_t}{N_t} - n_t(g_e + g_h) \\
\frac{\partial n_h}{\partial t} &= D_h \frac{\partial^2 n_h}{\partial z^2} - \frac{n_h}{\tau_h}\cdot\frac{n_t}{N_t} + g_h n_t
\end{aligned} \tag{4}$$

The release rates $g_e$ and $g_h$ of the carriers are described by the Shockley-Read model,[30]

$$\begin{aligned}
g_e &= \frac{1}{\tau_e}\cdot\frac{N_e}{N_t}\gamma_t exp\left(-\frac{E_t}{k_B T}\right), \\
g_h &= \frac{1}{\tau_h}\cdot\frac{N_h}{N_t}\gamma_t^{-1} exp\left(-\frac{E_g - E_t}{k_B T}\right),
\end{aligned} \tag{5}$$

and depend on the effective density of states of electrons and holes ($N_e$ and $N_h$), and on the position of trap level below the conduction band minimum $E_t$. The degeneracy factor $\gamma_t$ is assumed to be unity.

The total transient conductivity of photoexcited InGaAs layer defined by our model includes contributions from both electrons and holes and reads

$$\begin{aligned}
\Delta\sigma(\omega,\tau_p,\phi) = e_0 \int_0^L dz[&\mu_e(\omega) n_e(z,\tau_p,\phi) \\
&+ \mu_h(\omega) n_h(z,\tau_p,\phi)],
\end{aligned} \tag{6}$$

where $L = 3$ $\mu$m is the thickness of InGaAs layer. Note that the conductivity and free-carrier concentrations now depend on the excitation fluence $\phi$. The conductivity defined by Eq. (6) was convoluted with an instrumental function related to the noncollinear arrangement of the pump–probe experiment (Gaussian function in $\tau_p$ with a full-width-at-half-maximum of 1.5 ps). The result was fitted to the measured pump–probe scans of the transient conductivity; examples of the data and fits are shown in Fig. 6. The parameters for electrons ($\tau_{s,e}$ and $\mu_e$) and the initial concentration of electron-hole pairs, $n_0$, were estimated from the Drude spectral response described in the previous part, and they were kept fixed during the fit. The results of our fits are displayed in Table II.

The kinetics observed for each sample (A, B, and C) can be explained by taking into account an interplay of two processes: the trap filling and the carrier diffusion; these occur with different weights for each of the samples. The Shockley-Read terms Eq. (5) have not been found to have a significant impact on the observed carrier dynamics and can practically be neglected. We can thus infer that the trap level is sufficiently deep below the conduction band edge to prevent significant

Downloaded 10 May 2012 to 147.231.27.153. Redistribution subject to AIP license or copyright; see http://jap.aip.org/about/rights_and_permissions

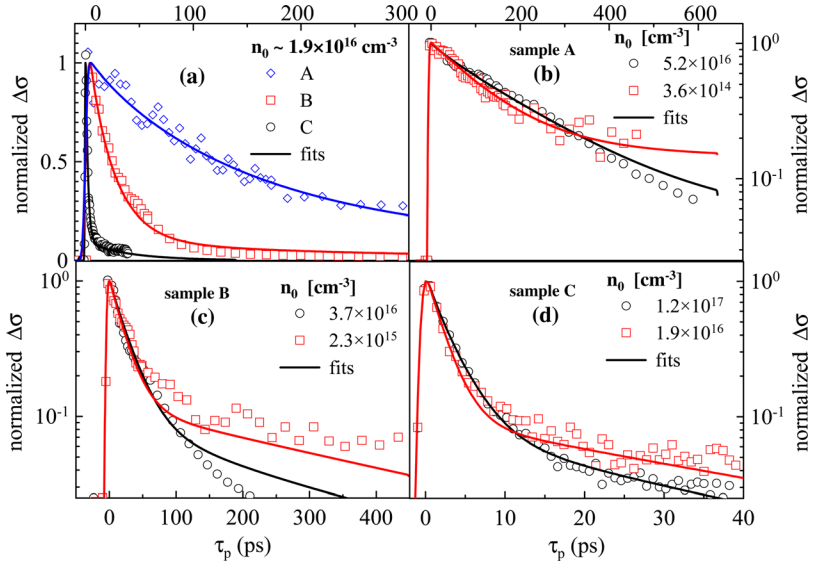


FIG. 6. Decay of the normalized ultrafast conductivity for samples A, B, and C and for several initial photocarrier densities. We plot the evolution of the photoconductivity at 1 THz [i.e., $\Delta\sigma(\omega_0 = 2\pi \times 10^{12}\mathrm{s}^{-1}, \tau_p)$] obtained following the method described at the end of the Sec. III. Note that the vertical scale for plots (b)–(d) is logarithmic. Experiment: symbols, fit: lines.

thermal activation of the trapped carriers, and we can roughly estimate $N_t \sim 0.3$ eV.

In the initial stage of the decay, the concentration of electrons and holes is similar, while the mobility of holes is about 5 to 12 times smaller than that of electrons (cf. Tables I and II). In this regime, the contribution of electrons to the total conductivity Eq. (6) is dominant and our interpretation of the measured spectral response displayed in Fig. 4 as that being essentially due to the contribution of electrons is correct. This regime holds approximately within $\tau_e$ or $2\tau_e$ for each sample. At later times, the contribution of holes may become comparable to that of electrons or even dominant and the determination of the hole mobility $\mu_h$ stems mainly from this part of the kinetics characterized by large pump-probe delays.

In sample A, where the concentration of traps $N_t$ is the lowest among the samples studied, the traps close to the sample surface can be efficiently filled for higher pump fluences within the electron lifetime. At the same time, as the carrier mobility is also high, these will have time to diffuse over the whole InGaAs layer thus making the available number of traps significantly higher. The effective decay time of the transient conductivity is then determined both by the lifetime of electrons and holes and by the carrier diffusion rate.

The concentration of the traps $N_t$ determined from the fits and shown in Table II scales approximately with the density of the host atom displacement defects. The concentration of the traps $N_t$ determined from the fits and shown in Table II scales approximately with the density of the host atom displacements $n_{host}$. The concentration of the traps is approximately one tenth of the density of the host atom displacements indicating that traps are constituted by several elementary atom displacements and also that some host atom displacements are probably not active for the capture of free carriers. In sample C, where the carrier lifetime is short, the diffusion of carriers cannot play a significant role in the carrier dynamics; however, the saturation of traps close to the surface occurs only for the highest pump fluences used. The kinetics observed are then governed by the depletion of the traps by the hole capture.

By analogy, the trap concentration in sample D, where a subpicosecond response time was found, should be of the order of nearly $10^{18}\,\mathrm{cm}^{-3}$. This means that neither diffusion nor trap filling should play a significant role for the pump fluence used (initial carrier concentration $<10^{17}\,\mathrm{cm}^{-3}$); the observed carrier lifetime of 300 fs then can be considered as that of free electrons.

The charge carrier mobility values and their lifetimes are summarized in Fig. 7. We observe quite good agreement with those measured using the optical excitation at 800 nm;[15] however, in that former work and also in previously published optical pump–probe experiments,[31] the lifetimes should be understood as effective carrier lifetimes depending on the dynamics of both electrons and holes. In the present work thorough pump fluence-dependent measurements allowed us to distinguish the role of electrons from that of holes. The mobility of holes decreases with the number of defects similarly as that of electrons; however, it was determined with a large experimental error and should be taken only as an estimation of its order of magnitude.

TABLE II. Summary of the values of parameters stemming from the kinetic model Eq. (4) of the decay of electron and hole populations.

| Sample | $n_{host}$ ($\mathrm{cm}^{-3}$) | $N_t$ ($\mathrm{cm}^{-3}$) | $\tau_e$ (ps) | $\tau_h$ (ps) | $\mu_h$ ($\mathrm{cm}^2\mathrm{V}^{-1}\mathrm{s}^{-1}$) |
|---|---|---|---|---|---|
| A | $2 \times 10^{16}$ | $3.1 \times 10^{15}$ | 110 | 290 | 1800 |
| B | $2 \times 10^{17}$ | $2.1 \times 10^{16}$ | 18 | 50 | 1000 |
| C | $2 \times 10^{18}$ | $0.9 \times 10^{17}$ | 2.1 | 10 | 550 |
| D | $2 \times 10^{19}$ | — | $\tau_c = 0.3$ | | — |

Downloaded 10 May 2012 to 147.231.27.153. Redistribution subject to AIP license or copyright; see http://jap.aip.org/about/rights_and_permissions

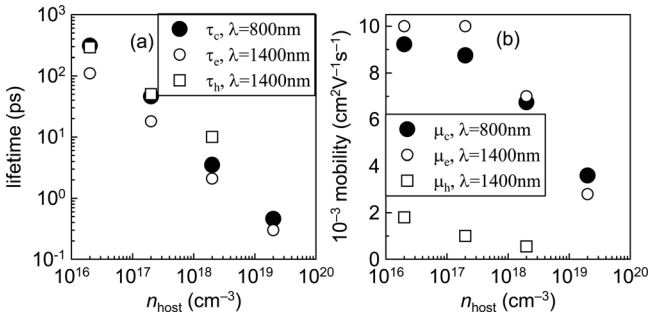


FIG. 7. Comparison of (a) carrier lifetimes [$\tau_c$ is effective carrier lifetime obtained in experiments with photoexcitation at 800 nm,[15] $\tau_e$ is the lifetime of electrons, and $\tau_h$ is the lifetime of holes] and (b) mobilities [$\mu_c$ refers to Ref. 15, $\mu_e$ is the mobility of electrons, and $\mu_h$ is the mobility of holes] as a function of host-atom displacement concentration. Closed symbols: excitation at 800 nm;[15] open symbols: excitation at 1400 nm.

## VI. CONCLUSION

We have investigated the dynamics of photogenerated carriers in $In_{0.53}Ga_{0.47}As$ films irradiated by heavy high-energy $Br^+$ ions using infrared pump–THz probe spectroscopy. To shed more light on the dynamics of both electrons and holes, the samples were excited at 1400 nm wavelength, and the pump fluences were varied within 2.5 orders of magnitude to achieve free carrier density from $5\times10^{14}$ to $1\times10^{17}$ cm$^{-3}$. The electron and hole lifetimes and mobilities were determined within a kinetic model, which accounts for the carrier diffusion within the InGaAs film and for the trap filling at high photocarrier densities. Both the carrier lifetimes and the density of traps are approximately proportional to the concentration of the host atom displacement defects. It was found that the $In_{0.53}Ga_{0.47}As$ film irradiated by the dose of $10^{12}$ cm$^{-2}$ exhibits simultaneously ultrashort electron lifetime (~300 fs) and very high electron mobility (2800 cm$^2$V$^{-1}$s$^{-1}$) which makes this material a promising candidate for the fabrication of THz emitters and detectors controlled by lasers operating at telecommunication wavelengths.

## ACKNOWLEDGMENTS

The financial support by the Czech Science Foundation (Project No 202/09/P099), by ASCR and its Grant Agency (Project Nos. AVOZ10100520 and A100100902), and by the Ministry of Education of the Czech Republic (Project No. LC-512) are acknowledged.

[1]A. Nahata, A. S. Weling, and T. F. Heinz, "A wideband coherent terahertz spectroscopy system using optical rectification and electro-optic sampling," Appl. Phys. Lett. **69**, 2321 (1996).
[2]A. Rice, Y. Jin, X. F. Ma, X. C. Zhang, D. Bliss, J. Larkin, and M. Alexander, "Terahertz optical rectification from ⟨110⟩ zinc-blende crystals," Appl. Phys. Lett. **64**, 1324 (1994).
[3]S. Gupta, M. Y. Frankel, J. A. Valdmanis, J. F. Whitaker, and G. A. Mourou, "Subpicosecond carrier lifetime in GaAs grown by molecular beam epitaxy at low temperatures," Appl. Phys. Lett. **59**, 3276 (1991).
[4]H. Němec, A. Pashkin, P. Kužel, M. Khazan, S. Schnüll, and I. Wilke, "Carrier dynamics in low-temperature grown GaAs studied by terahertz emission spectroscopy," J. Appl. Phys. **90**, 1303 (2001).
[5]N. Chimot, J. Mangeney, L. Joulaud, P. Crozat, H. Bernas, K. Blary, and J. F. Lampin, "Terahertz radiation from heavy-ion-irradiated In0.53Ga0.47As photoconductive antenna excited at 1.55 μm," Appl. Phys. Lett. **87**, 193510 (2005).
[6]M. Martin, J. Mangeney, P. Crozat, and P. Mounaix, "Optical phase detection in a 4-N,N-dimethylamino-4'-N'-methyl-stilbazolium tosylate crystal for terahertz time domain spectroscopy system at 1.55 μm wavelength," Appl. Phys. Lett. **97**, 111112 (2010).
[7]A. Schneider, M. Stillhart, and P. Günter, "High efficiency generation and detection of terahertz pulses using laser pulses at telecommunication wavelengths," Opt. Express **14**, 5376 (2006).
[8]A. Schneider, M. Neis, M. Stillhart, B. Ruiz, R. U. A. Khan, and P. Günter, "Generation of terahertz pulses through optical rectification in organic DAST crystals: Theory and experiment," J. Opt. Soc. Am. B **23**, 1822 (2006).
[9]A. Takazato, M. Kamakura, T. Matsui, J. Kitagawa, and Y. Kadoya, "Detection of terahertz waves using low-temperature-grown InGaAs with 1.56 μm pulse excitation," Appl. Phys. Lett. **90**, 101119 (2007).
[10]A. K. Azad, R. P. Prasankumar, D. Talbayev, A. J. Taylor, R. D. Averitt, J. M. O. Zide, H. Lu, A. C. Gossard, and J. F. O'Hara, "Carrier dynamics in InGaAs with embedded ErAs nanoislands," Appl. Phys. Lett. **93**, 121108 (2008).
[11]C. D. Wood, O. Hatem, J. E. Cunningham, E. H. Linfield, A. G. Davies, P. J. Cannard, M. J. Robertson, and D. G. Moodie, "Terahertz emission from metal-organic chemical vapor deposition grown Fe:InGaAs using 830 nm to 1.55 μm excitation," Appl. Phys. Lett. **96**, 194104 (2010).
[12]M. Suzuki and M. Tonouchi, "Fe-implanted InGaAs photoconductive terahertz detectors triggered by 1.56 μm femtosecond optical pulses," Appl. Phys. Lett. **86**, 163504 (2005).
[13]N. Chimot, J. Mangeney, P. Mounaix, M. Tondusson, K. Blary, and J. F. Lampin, "Terahertz radiation generated and detected by $Br^+$-irradiated $In_{0.53}Ga_{0.47}As$ photoconductive antenna excited at 800 nm wavelength," Appl. Phys. Lett. **89**, 083519 (2006).
[14]J. Mangeney, N. Chimot, L. Meignien, N. Zerounian, P. Crozat, K. Blary, J. F. Lampin, and P. Mounaix, "Emission characteristics of ion-irradiated $In_{0.53}Ga_{0.47}As$ based photoconductive antennas excited at 1.55 μm," Opt. Express **156**, 8943 (2007).
[15]J. C. Delagnes, P. Mounaix, H. Němec, L. Fekete, F. Kadlec, P. Kužel, M. Martin, and J. Mangeney, "High photocarrier mobility in ultrafast ion-irradiated $In_{0.53}Ga_{0.47}As$ for terahertz applications," J. Phys. D: Appl. Phys. **42**, 195103 (2009).
[16]S. E. Ralph, Y. Chen, J. Woodall, and D. McInturff, "Subpicosecond photoconductivity of $In_{0.53}Ga_{0.47}As$: Intervalley scattering rates observed via THz spectroscopy," Phys. Rev. B **54**, 5568 (1996).
[17]R. Dittrich and W. Schroeder, "Empirical pseudopotential band structure of $In_{0.53}Ga_{0.47}As$ and $In_{0.52}Al_{0.48}As$," Solid-State Electron. **43**, 403 (1999).
[18]J. P. Biersack and L. G. Haggmark, "A Monte Carlo computer program for the transport of energetic ions in amorphous targets," Nucl. Instrum. Methods **174**, 257 (1980).
[19]H. Němec, L. Fekete, F. Kadlec, P. Kužel, M. Martin, J. Mangeney, J. C. Delagnes, and P. Mounaix, "Ultrafast carrier dynamics in $Br^+$-bombarded InP studied by time-resolved terahertz spectroscopy," Phys. Rev. B. **78**, 235206 (2008).
[20]L. Joulaud, J. Mangeney, L. M. Lourtioz, P. Crozat, and G. Patriarche, "Thermal stability of ion-irradiated InGaAs with (sub-) picosecond carrier lifetime," Appl. Phys. Lett. **82**, 856 (2003).
[21]D. K. Schroder, *Semiconductor Material and Device Characterization*, 3rd ed. (Wiley, 2006), p. 97.
[22]L. Fekete, P. Kužel, H. Němec, F. Kadlec, A. Dejneka, J. Stuchlík, and A. Fejfar, "Ultrafast carrier dynamics in microcrystalline silicon probed by time-resolved terahertz spectroscopy," Phys. Rev. B **79**, 115306 (2009).
[23]D. A. Humphreys, R. J. King, D. Jenkins, and A. J. Moseley, "Measurement of absorption coefficients of $Ga_{0.47}In_{0.53}As$ over the wavelength range 1.0–1.7 μm," Electron. Lett. **21**, 1187 (1985); E. Zielinski, H. Schweizer, K. Streubel, H. Eisele, and G. Weimann, "Excitonic transitions and exciton damping processes in InGaAs/InP," J. Appl. Phys. **59**, 2196 (1985).
[24]P. Kužel, F. Kadlec, and H. Němec, "Propagation of terahertz pulses in photoexcited media: Analytical theory for layered systems," J. Chem. Phys. **127**, 024506 (2007).
[25]*Handbook Series on Semiconductor Parameters*, edited by M. Levinshtein, S. Rumyantsev, and M. Shur (World Scientific, Singapore, 1999), Vol. **2**, p. 62.
[26]H. Němec, F. Kadlec, S. Surendran, P. Kužel, and P. Jungwirth, "Ultrafast far-infrared dynamics probed by terahertz pulses: A frequency-domain approach. I. Model systems," J. Chem. Phys. **122**, 104503 (2005).
[27]H. Němec, F. Kadlec, C. Kadlec, P. Kužel, and P. Jungwirth, "Ultrafast far-infrared dynamics probed by terahertz pulses: A frequency-domain approach. II. Applications," J. Chem. Phys. **122**, 104504 (2005).

Downloaded 10 May 2012 to 147.231.27.153. Redistribution subject to AIP license or copyright; see http://jap.aip.org/about/rights_and_permissions

[28]D. C. Driscoll, M. P. Hanson, A. C. Gossard, and E. R. Brown, "Ultrafast photoresponse at 1.55 $\mu$m in InGaAs with embedded semimetallic ErAs nanoparticles," Appl. Phys. Lett. **86**, 051908 (2005).
[29]D. C. Driscoll, M. P. Hanson, and A. C. Gossard, "Carrier compensation in semiconductors with buried metallic nanoparticles," J. Appl. Phys. **97**, 016102 (2005).
[30]W. Shockley and W. T. Read, "Statistics of the recombinations of holes and electrons," Phys. Rev. **87**, 835 (1952).
[31]J. Mangeney and P. Crozat, "Ion-irradiated $In_{0.53}Ga_{0.47}As$ photoconductive antennas for THz generation and detection at 1.55 $\mu$m wavelength," C. R. Phys. **9**, 142 (2008).

Downloaded 10 May 2012 to 147.231.27.153. Redistribution subject to AIP license or copyright; see http://jap.aip.org/about/rights_and_permissions